Effects of Convective Asymmetries on Hurricane Intensity: A Numerical Study

Liguang Wu[1,2] and Scott A. Braun[2]

Submitted to *J. Atmos. Sci.*

Feb. 2003

[1]Goddard Earth and Technology Center, University of Maryland at Baltimore County, Baltimore, Maryland.

[2]Laboratory for Atmospheres, NASA Goddard Space Flight Center, Greenbelt, Maryland

Corresponding author address: Dr. Liguang Wu , NASA/GSFC, Code 912, Greenbelt, MD 20771

E-mail: liguang@agnes.gsfc.nasa.gov

ABSTRACT

The influence of the uniform large-scale flow, beta effect, and vertical shear of the environmental flow on hurricane intensity is investigated in the context of the induced convective or potential vorticity asymmetries with a hydrostatic primitive equation hurricane model. In agreement with the previous studies, imposing of one of these environmental effects can substantially weaken the simulated tropical cyclones. In response to the environmental influence, significant asymmetries develop with a structure similar to the spiral bands in real hurricanes, which are dominated by wavenumber-one components. The tendencies of the mean radial, azimuthal winds and temperature associated with the environment-induced convective asymmetries are evaluated respectively. The resulting asymmetries can effectively reduce hurricane intensity by directly producing the negative tendency of the mean tangential wind in the vicinity of the radius of maximum wind, and by weakening the mean radial circulation. The reduction effects are closely associated with the spiral structure of the induced asymmetries. The time lag observed between the imposition of the environmental influence and the resulting rise in the minimum central pressure is the time required for developing the spiral structure. This study also confirms the axisymmetrization process associated with the induced wavenumber-one components of potential vorticity asymmetries, but it exists only within the radius of maximum wind.

1 Introduction

Convective asymmetries that are embedded in highly axisymmetric rotating tropical cyclones (TCs) have been extensively studied for decades (e.g., Simpson 1952; Jordan 1952; Shea and Gray 1973; Lewis and Hawkins 1982; Jorgensen 1984; Bluestein and Marks 1987; Gall et al. 1998; Kuo et al. 1999; Reasor et al. 2000). The asymmetries have been explained in terms of internal gravity waves (Kurihara 1976; Willoughby 1978) and vortex Rossby waves (MacDonald 1968; Guinn and Schubert 1993; Montgomery and Kallenbach 1997). The existence of vortex Rossby waves associated with the potential vorticity (PV) gradient of the primary vortex of a TC has been recently verified through high-resolution numerical models by Chen and Yau (2001) and Wang (2002a and b). The asymmetries can accelerate the tangential wind of TCs through vortex axisymmetrization (Melander et al. 1987, Montgomery and Kallenbach 1997). A series of studies that focused mainly on tropical cyclogenesis have demonstrated the axisymmetrization process in a barotropic asymmetric balance model (Möller and Montgomery 1999), a three-dimensional (3D) quasigeostrophic model (Montgomery and Enagonio 1998), a 3D asymmetric balance model (Möller and Montgomery 2000), and a shallow water model (Enagonio and Montgomery 2001). Recently, Heymsfield et al. (2001) characterized the asymmetric structure of intense convection in Hurricane Bonnie (1998) using observations from the National Aeronautics and Space Administration (NASA) ER-2 and DC-8 aircraft and suggested that

the hurricane asymmetries may have played an important role in the intensification of the storm.

On the other hand, recent numerical studies suggest that asymmetries can reduce TC intensity. Peng et al. (1999) and Frank and Ritchie (1999, 2001) have investigated the TC intensity change due to the large-scale environmental influence (e.g., the beta effect, uniform environmental flows and vertical shear of the environmental flow). They showed that if one of these environmental factors is included in the numerical experiments, the resulting vortex is weaker than the one without environmental influence. Since all of the environmental effects result in significant asymmetries with the maximum amplitudes around the radius of maximum wind (RMW), it is suggested that, similar to the axisymmetrization process, the weakening of the simulated TCs may also be associated with the resulting asymmetric circulation. It is also consistent with the notion that intense hurricanes tend to be rather symmetric, whereas less intense hurricanes have their convection organized in asymmetric spiral bands (Willoughby et al. 1984).

Eddy fluxes of heat and momentum associated with the large-scale circulation can contribute to the symmetric circulation of TCs. During the formative stage, as shown by Pfeffer (1958), Challa and Pfeffer (1980) and Challa et al. (1998), the large-scale environmental eddy fluxes can induce a secondary radial circulation with outflow in the upper troposphere and inflow in the lower troposphere, thereby drawing

moisture into the region, organizing the convection and providing lifting necessary to set off conditional instability. Bosart et al. (2000) attributed the rapid intensification of hurricane Opal (1995) to the eddy fluxes of heat and momentum associated with an approaching trough. However, Persing et al. (2002) and Möller and Shapiro (2002) found that the approaching trough in the case of Opal contributed little to the intensification.

In this study, the role of hurricane asymmetries is examined in a series of idealized numerical experiments with a full-physics model by focusing on how the convective asymmetries induced by simple large-scale flows or the beta effect can affect the TC intensity. The primary purpose here is to understand the underlying physical processes responsible for the weakening of TCs that occurs when they are subjected to simple environmental influences, as shown by Peng et al.(1999) and Frank and Ritchie (1999, 2001). The asymmetries are associated with highly idealized large-scale flows and not with large-scale circulations such as troughs, as discussed by Challa et al. (1998). The asymmetries are also different from the ones in the studies by Montgomery and coworkers, in which the asymmetries were specified as initial conditions and meant to approximate vorticity sources associated with asymmetric convection.

This paper is organized as follows. In section 2, we summarize the numerical model used in this study and the numerical experiments. Section 3 describes the re-

sponse of TCs to the imposed environmental influence, including both the symmetric and asymmetric structure. In section 4, the contributions of the resulting asymmetric circulations to the TC intensity change are evaluated. In section 5, some relevant issues related TC intensity change are discussed based upon the results in this study. Conclusions are provided in section 6.

2 Numerical model and experimental design

In previous studies, the numerical models used were diverse in terms of their resolution and the complexity of the model physics. For example, the horizontal grid spacings used by Peng et al. (1999) and Wu (1999) were 0.5^o and 25 km, respectively, whereas the simulations by Frank and Ritchie were performed with a grid spacing of 15 km in 1999 and 5 km in 2001. Peng et al. and Wu used the Kuo scheme (Kuo 1974) for cumulus physics, while Frank and Ritchie applied the cumulus parameterization of Betts and Miller (1986) to the 15 km-simulations and an explicit moisture scheme to the 5 km experiments. The simulated responses of TCs to imposed large-scale flows have been similar in all of these experiments. Therefore, the first-order effects of the environmental flows are phenomena that can be qualitatively simulated in a numerical model with relatively coarse resolution and simple physics.

In this study, the numerical model is the same as that used by Wu and Wang (2000). The cumulus convection is parameterized with Kuo's (1974) cumulus scheme

and the calculations of horizontal and vertical turbulent fluxes of momentum, heat, and moisture follow Smagorinsky et al. (1965) and Louis (1979), respectively. The details of the model and its capability in simulating the motion and evolution of baroclinic TCs in the presence of diabatic heating has been documented by Wu and Wang (2000, 2001a and b). The model consists of 201 × 201 grid points with a uniform horizontal spacing of 25 km and 16 vertical layers.

This study examines four numerical experiments that are designed to investigate the various environmental factors: the planetary vorticity gradient (beta effect), uniform zonal environmental flow and vertical shear of the mean zonal flow. All the experiments begin with the same initially symmetric baroclinic vortex. The tangential wind profile of the initial cyclonic vortex is shown in Fig.1a, with a maximum wind of 25 ms^{-1} at a radius of 100 km. The sea surface temperature (SST) remains horizontally uniform and fixed (29.5^oC) throughout the integration. The first experiment (E0) is a control run on an f-plane without environmental flow. In agreement with Wu and Wang (2000), the vortex doesn't move and maintains its symmetric structure throughout the integration period of 96h. It develops into a strong hurricane with a minimum surface pressure of 902.5 mb at 96h. As shown in Fig.1b, the radius of maximum wind (RMW) slightly tilts outward with height and a warm core of about 10^oC develops at about 250 mb. The maximum wind appears at about 900 mb due to friction. Therefore, the model produces a simulated hurricane with

realistic general structure.

As shown in Table 1, the other three experiments are performed under the influence of vertical shear of the zonal environmental wind (E1), the beta effect (E2) and uniform zonal mean flow (E3), respectively. The large scale environmental influence is imposed at the beginning of the integration. The imposed wind, consisting of either mean zonal flow or vertically sheared flow, can significantly affect the TC structure and even prevent development from occurring if the flow or shear is excessively strong. Therefore, we select a moderate uniform flow of -4 $m\ s^{-1}$ in E3 and a moderate vertical shear that decreases with height from -4 $m\ s^{-1}$ at the surface to 0 $m\ s^{-1}$ at the top of the model in E1.

3 Response of TC structure to environmental effects

a) TC intensity

Figure 2 shows the evolution of the maximum wind at the lowest model level and the central pressures for all of the simulations. The run with zero-mean flow (E0) is the most intense simulation. All the simulated TCs developed in a similar manner. That is, the first 36 h of rapid intensification was followed by a period

of slower intensification and finally by a quasi-steady state. The major changes in TC intensity associated with the different large-scale environments are most evident after 36 h of integration although their influence is imposed at 0h. Such a delayed response of the storm's intensity has been noticed by Frank and Ritchie (2001) using the nonhydrostatic Pennsylvania State University-National Center for Atmospheric Research fifth-generation Mesoscale Model.

In E1, the vortex reached a central surface pressure of 910.6 mb at 96h. Compared with case E0, the central surface pressure increased by about 8 mb as a result of the imposed vertical shear of the environmental flow. Case E2 was run on a beta plane without environmental flow. The vortex only attained a central surface pressure of 937.2 mb at 96h, a rise of about 35 mb compared to E0. In E3, with a uniform easterly environmental flow of -4 $m\ s^{-1}$, the storm's intensity was reduced by about 21 mb at 96 h. Consistent with the study by Peng et al. (1999), introduction of either uniform zonal environmental flow, vertical shear of the zonal environmental flow, or the beta effect weakened the TCs.

Frank and Ritchie (2001) found that in a similar easterly-flow simulation the storm was slightly more intense than the zero-flow case. They argued that a new physical process may be responsible for the intensity difference. Although significant asymmetries developed in the eyewall structure in their easterly-flow case, the evaporation of rainfall and resolvable-scale downdrafts made the boundary layer cooler in

their zero-flow case because the storm didn't move. This process is not included in the current study, as well as in the study by Peng et al. (1999), since downdrafts are not included in the cumulus parameterization.

b) Symmetric structure

Figure 3 shows the vertical structure of the symmetric tangential winds at 96 h for E1, E2, and E3. Careful examination of the structures of the simulated TCs indicates that the imposed moderate environmental flows still significantly modify the symmetric structures of the simulated TCs. Compared to Fig. 1b (Note the contour interval difference in Fig. 3), the weakening of the maximum wind at about 900 mb in E2 and E3 is apparent. Despite the coarse horizontal resolution, we can find that the RMW are slightly shifted outward in response to the large-scale environmental effects in these two experiments. In E2, a relatively strong anticyclonic circulation appears at the upper levels. Figure 4 shows the deviations of the symmetric tangential wind from E0 at 96 h. The decrease in the tangential wind extends through all levels in E2 and E3, mainly in the vicinity of the RMW. Note that the shift of the RMW cannot account for the wind reduction because it extends to a radius of 200 km. In E1 the reduction of the tangential wind primarily occurs at upper levels. It is interesting to note that a relatively smaller reduction (E2 and E3) or even increase (E1) in the mean tangential wind appears around 700-800 mb in the vicinity of the RMW.

Consistent with the structure of a mature hurricane, as shown in Fig. 1c, the inflow and outflow are primarily located in the lower and upper layers. A secondary inflow maximum can be found at about 300 mb. Figure 5 shows the deviations of the symmtric radial wind of E1, E2 and E3 from that in E0 at 96 h. In the presence of the environmental influence, the outflows in the upper layer are significantly reduced in all of the experiments. In addition, the inflows in the boundary layers of E2 and E3 are also reduced. The reduction in both the inflow and outflow indicates the weakening of the symmetric radial circulation. The positive anomalies around 300 mb in Fig. 5 are associated with the significant weakening of the secondary inflow maximum there.

Figure 6 shows the temperature anomalies with respect to the environment at 96 h. The magnitudes of the maximum temperature anomalies are almost the same in all the experiments (about 12°C). However, the heights of the warm cores are generally lower than in E0 as a result of the weakening effects of the specified environments. The warm cores are located around 250 mb in E0 and E1, whereas they are located about 350 mb in E3 and 450 mb in E2. Consistent with hydrostatic balance, the lowest central pressures are found in cases where the warm anomalies are located at the highest heights. Thus, Fig. 6 suggests that, compared to E0, the reduced intensities in E2 and E3, as measured by the minimum central pressure, are associated with a lowering of the warm anomaly and not so much as a result of a

reduction in its magnitude.

c) Asymmetric structure

In this study, the vortex center is defined as the location of maximum PV (e.g., Wu and Wang 2000). In order to minimize the effects of the coarse grid spacing, the PV is interpolated to finer grids. In studies of TC motion, Wu and Wang (2000, 2001a and 2001b) have shown that the resulting asymmetric circulation is generally realistic. The TC center location is only determined at the lowest model level. Because of the moderate environmental effects, the variation of the center location with height is actually very small from the surface to 300 mb.

A common feature in the three experiments (E1, E2 and E3) is the significant asymmetries that develop as a result of the imposed environmental effects. Figure 7 shows the evolution of the resulting asymmetries in terms of PV at level 14 (900mb) for E1, E2 and E3. According to May et al. (1994) and May and Holland (1999), local maxima of atmospheric PV are closely associated with convective asymmetries. For this reason, we use the PV asymmetries as a proxy for enhanced convection. As indicated by the small circles, after the initial development stage (12 h), the asymmetries show maxima of PV that spiral cyclonically toward the center, occasionally with two maxima that are connected by relatively weak PV (Fig. 7). Willoughby et al. (1984) provided a schematic diagram of radar reflectivity in TCs that included convective

structures outside of the core. They showed that high reflectivity in the eyewall extended outward cyclonically. In this sense the resulting PV anomaly pattern bears a remarkable resemblance to the spiral bands observed in real hurricanes.

The generation of the asymmetries can be attributed to several mechanisms that have been discussed in previous studies. Shapiro (1983) suggested that the asymmetries in friction tend to cause a wavenumber one asymmetry in convergence, in which the maximum eyewall convergence occurs ahead and to the right of the storm motion vector for slow to moderate moving TCs. In the three experiments, the TCs generally moved westward (E1, E3) or northwestward (E2), and the maximum convergence (not shown) occurs on western and northwestern sides. As shown in Fig. 7, this mechanism can account for the primary patterns of the resulting positive PV anomalies.

Peng et al. (1999) investigated the development of TC asymmetries in the context of the surface frictional wind. This mechanism may also contribute to the generation of resulting positive PV anomalies. In the presence of an easterly flow, for example, the tangential wind on the northern side and the inward radial wind on the eastern side of the vortex are increased. As a result, an easterly flow is expected to generate maximum surface flux in the northeastern part of the vortex. Because of cyclonic advection by the tangential wind, the asymmetries actually are observed on the northern or northwestern side, as seen in E1 and E3.

In E1 and E2, the effects associated with vertical shear also play a role. Frank and Ritche (1999) suggested that convection tends to be enhanced on the downshear-left side. In E2 the ventilation flow associated the beta gyres tends to decrease with height (Wang and Li 1992) with the shear vector directed to the southeast. The enhanced convection (PV) appears on the eastern or northeastern side, which is more obvious at 12 h and 96 h (Fig. 7). In E1 the westerly shear vector also suggests that convection is enhanced on the northern side.

Jones (1995) showed that the tilt of a TC can lead to significant asymmetric structure of TCs. Because of diabatic heating effects, the vertical tilt of the simulated TCs in the current study is very small (within a grid point) from the surface to 300 mb. In this case, it seems that the mechanism associated with vertical tilt plays a minor role in the generation of the asymmetries.

Using the high-resolution PSU-NCAR MM5, Chen and Yau (2001) analyzed the spiral PV bands and found that the propagation properties of the PV bands were consistent with predictions of vortex Rossby wave theory. In the current study, despite the relatively coarse horizontal resolution, the PV gradient associated with the primary symmetric vortex satisfies the necessary conditions for the development of vortex Rossby waves. Therefore, the asymmetric PV anomalies may be associated with vortex Rossby waves.

4 Contribution of convective asymmetries

Eliassen's (1952) symmetric balanced formulation has been used to understand the influence of eddy fluxes associated with the large-scale circulation on the formation and intensification of hurricanes (Pfeffer 1958). In this dynamical framework, a hurricane is treated as a stable symmetric vortex and never deviates far from hydrostatic or gradient balance. The contributions from eddy fluxes of heat and momentum associated with the asymmetric circulation are related to the deduced secondary radial circulation. In order for the derived diagnostic equation to be solvable, the equation must be elliptic (Möller and Shapiro 2002). The necessary condition is that the PV for the symmetric vortex be positive. However, negative PV in the outflow layer is a typical feature of hurricanes. For this reason, we directly assess the contributions of the eddy fluxes associated with the asymmetries to the tendencies of radial and tangential winds and potential temperature. In cylindrical coordinates with an origin at the center of the TC, we can write these equations describing the eddy contributions as follows

$$(\frac{\partial \overline{u}}{\partial t})_{eddy} = -(\frac{\overline{u'^2} - \overline{v'^2}}{r} + \frac{\partial \overline{u'^2}}{\partial r} + \frac{\partial \overline{u'\omega'}}{\partial p}), \tag{1}$$

$$(\frac{\partial \overline{v}}{\partial t})_{eddy} = -(\frac{2\overline{u'v'}}{r} + \frac{\partial \overline{u'v'}}{\partial r} + \frac{\partial \overline{v'\omega'}}{\partial p}), \tag{2}$$

$$(\frac{\partial \overline{\theta}}{\partial t})_{eddy} = -(\frac{\overline{u'\theta'}}{r} + \frac{\partial \overline{u'\theta'}}{\partial r} + \frac{\partial \overline{\theta'\omega'}}{\partial p}), \tag{3}$$

where t, r, λ, and p are time, radius, azimuth, and pressure, respectively; $\overline{u}$, $\overline{v}$ and $\overline{\theta}$ are the azimuthal mean winds and potential temperature; and $u\prime$, $v\prime$, $w\prime$ and $\theta\prime$ are the asymmetric radial and tangential, vertical winds and potential temperature components, respectively. Equations 1-3 indicate that the convective asymmetries can affect the tendencies of the tangential and radial winds and the potential temperature of the mean symmetric circulation through the terms on the right hand side.

In order to evaluate the effects of the eddy fluxes on the tendencies of the mean tangential and radial winds and the mean potential temperature, the model output is converted into an tangential coordinate system centered on the TCs. Since some uncertainty may be introduced as a result of inaccuracies of the center locations at one time, terms associated with the eddy fluxes are calculated each hour and averaged over the period from 24 h to 96 h for the three experiments. The time-averaged calculations are more likely to represent the persistent physical processes as compared to calculations from a single time step.

Figure 8 shows the 72h-mean contribution from the asymmetric circulation to the tendency of the mean radial wind in E1, E2 and E3, respectively. The contribution, primarily confined to the vicinity of the RMW, affects the TC intensity in two ways. First, a positive center is located around the RMW near the surface that tilts outward with height, and a center of negative tendencies appear at about 850 mb. Since the transition of the low-level inflow and outflow occurs at 850 mb, the tendency

of the radial wind indicates that the inflow and outflow are reduced because of the eddy momentum flux. In other words, an extra radial circulation is induced that is contrary to the mean secondary radial circulation, as indicated schematically in the figure, and acts to reduce the TC intensity. Note that the amplitude of tendency in E2 is weaker than in E1 and E3. Second, as shown in Fig. 8, the eddy flux associated with the asymmetric circulation induces significant negative tendencies around 200 mb. Since the locations of the negative tendencies coincide with the outflow layer (see Fig. 1c), these negative tendencies will effectively weaken the TC intensity by reducing the mean outflow and the convection of the eyewall.

The contributions discussed above may not directly affect the symmetric radial flow since they can be counteracted by other terms in the momentum equation. However, if the symmetric circulation is balanced and symmetrically stable, Molinari et al. (1993) found that the unbalanced portion of the secondary circulation was a simple modification of the balanced circulation in response to the gradient imbalances caused by the eddy fluxes and can affect TC intensity. Comparing Fig. 8 with Fig. 5, shows that the induced asymmetric TC circulation directly affects the mean radial circulation, especially in the outflow layer, since the changes in the radial winds (Fig. 5) are roughly similar to the patterns of the resulting tendencies (Fig. 8).

Figure 9 shows the 72h-averaged contribution from the induced asymmetries to the mean tangential wind. Significant negative centers of the tendencies can be

found at lower levels and upper levels. When compared to Fig. 3, the low-level negative centers are roughly located in the core of the maximum winds, indicating that the negative tendencies can substantially reduce the TC intensity. In addition, the reduced tangential winds at the lowest level lead to a decrease of the surface fluxes that are crucial to maintaining the TC intensity (Emanuel 1987). The mean tangential wind tendency is not uniform in the vertical. The vertical distribution suggests that, if we consider only the influence of the contribution of the mean azimuthal momentum flux, the tangential wind tends to be reduced at lower and upper levels, while it is enhanced at middle levels. The tangential winds shown in Fig. 4 are consistent with the tangential wind tendencies in that there is a relatively smaller reduction at middle levels. This result suggests a direct influence of the mean azimuthal momentum flux.

It is generally believed that most hurricanes fail to reach their maximum potential intensity (MPI) primarily because of the wind-induced sea surface cooling, downdrafts or the inhibiting effect of vertical wind shear. Previous studies (Gray 1968; Anthes 1982; Frank and Ritchie 2001) suggested that shear can inhibit intensification through differential advection of the upper warm anomaly from the low-level circulation, thereby raising the pressure at lower levels according to hydrostatic balance. Figure 10 shows the temperature deviations in E1, E2 and E3 from that in E0 at 96 h. The temperature changes in the eye are qualitatively similar in all three cases. Consistent with the weakening of the simulated TCs, the air in the eye warmed up

at lower and middle levels and cooled down at upper levels. Since no environmental shear was involved in case E3, these temperature deviations are not caused by the differential advection associated with vertical shear. Figure 11 shows the tendency of the mean potential temperature caused by the asymmetries. Comparing Fig. 11 with Fig. 10 suggests that the temperature deviations are not the direct result of the mean eddy heat flux on the right hand side of (3). In Fig. 11 , the negative tendencies in the eyewall regions are apparent in all three cases, but Fig. 10 indicates that these negative temperature tendencies didn't significantly modify the temperature in the eyewall. We suggest that the temperature deviations result from an adjustment of the temperatures , via thermal wind balance, to changes in the primary circulation toward which the eddy fluxes contribute.

Only a small part of the contributions associated with the asymmetric circulation actually affects the TC intensity. As shown in Fig. 9, the tendency of the mean tangential winds can be as large as 150 ms^{-1} day^{-1}, but the difference in mean tangential winds shown in Fig. 3c is only about 12 ms^{-1}. The temperature tendencies shown in Fig. 10 can be 8^o C day^{-1}, whereas the actually cooling is only a few degree. It is apparent that most of the contributions from the asymmetric circulation are balanced by budget terms in the governing equations that are associated with contributions by the symmetric circulation.

5 Discussion

Previous studies on the effects hurricane rainbands have focused on the weakening of eyewall convection caused by downdrafts. Powell (1990) found that mesoscale descent and occasional convective-scale penetrative downdrafts were present on the inner side of outer convective rainbands. As a result, strong rainbands can act as a barrier for inflow in the hurricane boundary layer. In the case with concentric rings of convection, a rainband outside the eyewall constricts and prevents subcloud air from reaching the eyewall and leads to the dissipation of the original eyewall and an eyewall replacement (Shapiro and Willoughby 1982; Willoughby et al. 1982). For rainbands composed primarily of stratiform downdrafts, precipitation may be produced by mesoscale melting and evaporation within the stratiform reflectivity regions (Powell 1990), leading to the weakening of the eyewall convection, or eyewall breakdown.

Since the Kuo cumulus scheme does not include convective downdrafts, their effects are not responsible for the weakening. In addition, the relatively coarse grid resolution used in our simulations severely limits the model's ability to simulate eyewall replacement cycles. In the present study, we propose that the momentum fluxes associated with the resulting convective asymmetries can reduce TC intensity by weakening both mean radial circulation and tangential winds at lower and upper levels.

As discussed in section 3, although the PV asymmetries develop by 12 h (Fig. 7), the weakening of the simulated TCs is not apparent until 36 h (Fig. 2), indicating a time lag between the imposition of the large-scale flows and their effects. Similar time lags were also found by Frank and Ritchie (2001). Careful examination of Fig. 7 shows that the spiral structure of the asymmetries was not well developed at the early stage of integration. Figure 12 shows the evolution of the tendency of the mean tangential wind at 900 mb in E1, E2 and E3, respectively. We can see that the contribution of the asymmetries is not significant until 36 h. The evolution of the tendency of the mean radial wind is similar (not shown). It is suggested that the time lags may be associated with the development of the spiral structure of the asymmetries.

Figure 13 shows the asymmetric wind fields associated with the PV asymmetries in E3. At 700 mb (the upper panel), the uniform environmental flow is distorted as a result of its interaction with the TC. The flow diverages as it approaches the TC and converges as it leaves. On the other hand, at 900 mb (the lower panel), a pair of strong gyres is present with centers at the RMW. The right panels of Fig. 13 show the corresponding tendency of mean tangential wind associated with the wind fields. At 700 mb (the upper panels), a large positive tendency occurs near the RMW whereas at 900 mb negative tendencies occur just inside the RMW and the significant positive tendencies occur near the center of the vortex. This figure suggests that the influence

of the momentum flux is closely associated with the pattern of the asymmetric wind fields.

In order to demonstrate the importance of the spiral structure in the axisymmetrization process, we can assume that the stream-function ($\psi(r,\lambda,t)$) of the resulting wavenumber-one circulation takes the form

$$\psi(r,\lambda,t) = \phi(r,t)cos(\alpha(r) - \lambda), \tag{4}$$

where $\phi(r,t)$ and $\alpha(r)$ are the amplitude and initial phase measured counterclockwise. By neglecting the divergence, we have $u = -\frac{\partial\psi}{r\partial\lambda}$, $v = \frac{\partial\psi}{\partial r}$. Here we only take the the tendency of the mean tangential wind associated with the asymmetries as an example. A similar analysis can be applied to the tendency of the mean radial wind. Since the tendency of the mean tangential wind is dominated by the first two terms in (2), it can be written as

$$-(\frac{\partial\overline{u'v'}}{\partial r} + 2\frac{\overline{u'v'}}{r}) = -\frac{\partial\alpha}{\partial r}(\frac{\phi^2}{2r^2} + \frac{\phi}{2r}\frac{\partial\phi}{\partial r}), \tag{5}$$

where the spiral band is approximated as an equiangular spiral, $\frac{\partial^2\alpha}{\partial r^2} = 0$ (Willoughby et al. 1984); the term associated with the vertical momentum flux is not included. Since the amplitude of the stream-function is maximum at the RMW, $\frac{\partial\phi}{\partial r} > 0$ within the RMW. As the asymmetries spiral outward cyclonically ($\frac{\partial\alpha}{\partial r} < 0$), the tendency of the mean tangential wind is positive in the eye, as shown in Fig. 12. The factor of $\frac{1}{r}$ in (5) suggests that the maximum occurs near the vortex center.

The effects of the vortex asymmetries discussed here generally agree with the axisymmetrization mechanism discussed by Montgomery and coworkers (e.g., Montgomery and Enagonio 1998; Möller and Montgomery 2000; Enagonio and Montgomery 2001). At the early stages of TC development, they found that vortex intensification proceeds by ingestion of like-sign PV anomalies into the parent vortex and expulsion of opposite-sign PV anomalies during the axisymmetrization process. As shown in Fig. 12, however, since such an axisymmetrization process only occurs within the RMW, its influence will be very limited until significant asymmetries develop.

6 Summary

A hurricane's weakening resulting from the large-scale influences has been observed in many previous studies (e.g., Peng et al., 1999; Frank and Ritche 1999, 2001; Wu 1999). In order to understand the phenomenon, idealized experiments were designed to include uniform environmental flow, the beta effect, and vertical shear. In order to focus on the impacts of the convective asymmetries, the effects of the convective downdrafts and the eyewall replacement cycle on TC intensity are excluded by using a relatively coarse-resolution model with a cumulus scheme that doesn't include downdrafts.

The simulated effects of the environmental influence on TC intensity are very similar to the previous studies (Peng et al., 1999; Frank and Ritche 1999, 2001; Wu

1999). In response to the environmental influence, in addition to the changes in the TC intensity and symmetric structure, significant asymmetries develop, primarily with wavenumber-one components. The resulting asymmetries resemble the spiral bands in terms of their structure. The effects of the induced asymmetries on TC intensity are investigated in the context of the associated fluxes of momentum and heat. The asymmetries reduce the simulated TC intensity by directly inducing a negative tendency of the mean tangential wind in the vicinity of the RMW and by weakening the mean radial circulation. The reduced tangential winds lower the height of the warm anomaly through thermal wind balance, thereby increasing the minimum central pressure relative to the case without environmental influence. The axisymmetrization process that has been found in adiabatic experiments with specified PV patches by Montgomery and coworkers can be identified only within the RMW.

The effects of the convective asymmetries on TC intensity are closely associated with the development of their spiral structure. The time lag between the imposition of the large-scale forcing and the resulting rise in the minimum central pressure is the time required for the development of the spiral structure of the asymmetric circulation. It is found that the contribution from the asymmetric circulation is very small until the spiral structure is well developed.

As discussed in the last section, several physical mechanisms have been proposed to understand the change in the hurricane intensity. The numerical experiments

in this study are designed to focus on the effects of the resulting asymmetries, especially the ones induced by large-scale flows. The environmental effects were designed to be moderate and idealized in order to facilitate our analysis, but may underestimate the effects of other physical processes. For this reason, further investigation of various physical mechanisms responsible for TC intensity change is ongoing through the simulation of Hurricane Erin(2001) with the more sophisticated MM5 model.

Acknowledgments.

REFERENCES

Bluestein, H. W., and F. D. Marks Jr., 1987: On the structure of the eyewall of Hurricane Diana (1984): Comparison of radar and visual characteristics. *Mon. Wea. Rev.*, **115**, 2542-2552.

Bosart, L. E., C. S. Velden, W. E. Bracken, J. Molinari, and P. G. Black, 2000: Environmental influences on the rapid intensification of Hurricane Opal (1995) over the Gulf of Mexico. *Mon. Wea. Rev.*, **128**, 322-352.

Chall, M., and R. L. Pfeffer, 1980: Effects of eddy fluxes of angular momentum on the model hurricane development. *J. Atmos. Sci.*, **37**, 1603-1618.

—, —, Q. Zhao, and S. W. Chang, 1998: Can eddy fluxes serve as a catalyst for hurricane and typhoon formation? *J. Atmos. Sci.*, **55**, 2201-2219.

Chen, Y., and M. K. Yau, 2001: Spiral bands in a simulated hurricane. Part I: Vortex Rossby wave verification. *J. Atmos. Sci.*, **58**, 2128-2145.

Eliassen, A., 1952: Slow termally or fricyionally controlled meridional circulation in a circulare vortex. *Astropyys. Norv.*, **5**, 1960.

Enagonio, J., and M. T. Montgomery, 2001: Tropical cyclogenesis via

convectively forced vortex Rossby waves in a shallow water primitive equation model. *J. Atmos. Sci.*, **58**, 685-705.

Frank, W. M., and E. A. Ritchie, 1999: Effects on environmental flow upon tropical cyclone structure. *Mon. Wea. Rev.*, **127**, 2044-2061.

—, and —, 2001: Effects of vertical wind shear on the inetnsity and structure of numerically simulated hurricanes. , *Mon. Wea. Rev.*, **129**, 2249-2269.

Gall, R., J. Tuttle, and P. Hildebrand, 1998: Small-scale spiral bands observed in Hurricanes Andrew, Hugo, and Erin. *Mon. Wea. Rev.*, **126**, 1749-1766.

Guinn, T., and W. H. Schubert, 1993: Hurricane spiral bands. *J. Atmos. Sci.*, **50**, 3380-3404.

Heymsfield, G. M., J. B. Halverson, J. Simpson, L. Tian, and T. P. Bui, 2001: ER-2 Doppler radar investigations of the eyewall of Hurricane Bonnie during the Convection and Moisture Experiment-3. *J. Appl. Meteor.*, **40**, 1310-1330.

Jones, S. C., 1995: The evolution of vortices in vertical shear. Part I: Initially barotropic vortices. *Quart. J. Roy. Meteor. Soc.*, **121**, 821-851.

Jordon, C. L., 1952: On the low-level structure of typhoon eye. *J. Meteor.*, **9**, 285-290.

Jorgensen, D. P., 1984: Mesoscale and convective-scale characteristics of mature hurricanes. Part II: Inner core structure of Hurricane Allen (1980). *J. Atmos. Sci.*, **41**, 1287-1311.

Kuo, H. C., R. T. Williams, and J.-H. Chen, 1999: A possible mechanism for the eye rotation of Typhoon Herb. *J. Atmos. Sci.*, **56**, 1659-1673.

Kuo, H. L., 1974: Further studies of the parameterization of the influence of cumulus convection on large-scale flow. *J. Atmos. Sci.*, **31**, 1232-1240.

Kurihara, Y., 1976: On the development of spiral bands in a tropical cyclone. *J. Atmos. Sci.*, **33**, 940-958.

Lewis, B. M., and H. F. Hawkins, 1982: Polygonal eye walls and rainbands in hurricanes. *Bull. Amer. Meteor. Soc.*, **63**, 1294-1300.

Loise, J. F., 1979: A parametric model of vertical eddy fluxes in the atmosphere. *Bound.-Layer Meteror.*, **17**, 746-756.

MacDonald, N. J., 1968: The evidence for existence of Rossby-type waves in the hurricane vortex. *Tellus*, **20**, 138-150.

May, P. T., 1996: The Organization of convection in the rainbands of

tropical cyclone Laurence. *Mon. Wea. Rev.*, **124**, 807-815.

May, P. T., and G. J. Holland, 1999: The role of potential vorticity generation in tropical cyclone rainbands. *J. Atmos. Sci.*,**56**, 1224-1228.

Melander, M. V., J. C. McWilliams, and N. J. Zabusky, 1987: Axisymmetrization and vorticity-gradient intensification of an ioslated two-dimensional vortex through filamentation. *J. Fluid Mech.*, **178**, 137-159.

Möller, J. D., and M. T. Montgomery, 1999: Vortex Rossby-waves and their influence on hurricane intensification in a barotropic model. *J. Atmos. Sci.*, **56**, 1674-1687.

—, and — , 2000: Tropical cyclone evolution via potential vorticity anomalies in a three-dimensional balanced model. *J. Atmos. Sci.*, **57**, 3366-3387.

—, and L. S. Shapiro, 2002: Balanced contributions to the intensification of Hurricane Opal as diagnosed from a GFDL model forecast. *Mon. Wea. Rev.*, **130**, 1866-1881.

Montgomery, M. T., and R. J. Kallenbach, 1997: A theory for vortex Rossby-waves and its application to spiral bands and intensity changes in hurricanes. *Quart. J. Roy. Meteor. Soc.*, **123**, 435-465.

—, and J. Enagonio, 1998: Tropical cyclogenesis via convectively forced vortex Rossby waves in a three-dimensional quasigeostrophic model. *J. Atmos. Sci.*, **55**, 3176-3207.

Peng, M. S., B.-F. Jeng, and R. T. Williams, 1999: A numerical study on tropical cyclone intensification. Part I: Beta effect and mean flow effect. , *J. Atmos. Sci.*, **56**, 1404-1423.

Persing, J., M. T. Montgomery, and R. E. Tuleya, 2002: Environmental interactions in the GFDL hurricane model of Hurricane Opal. *Mon. Wea. Rev.*, **130**, 298-317.

Pfeffer, R. L., 1958: Concerning the mechanics of hurricanes. *J. Meteor.*, **15**, 113-120.

Powell, M., 1990: Boundary layer structure and dynamics in outer hurricane rainbands. Part II: Downdraft modification and mixed layer recovery. *Mon. Wea. Rev.*, **118**, 918-938.

Reasor, P. D., M. T. Montgomery, F. D. Marks Jr., and J. F. Gamache, 2000: Low-wavenumber structure and evolution of the hurricane inner core observed by airborne dual-Doppler radar. *Mon. Wea. Rev.*, **128**, 1653-1680.

Shea, D. J., and W. M. Gray, 1973: The hurricane inner core region. I:

Symmetric ans asymmetric structure. *J. Atmos. Sci.*, **30**, 1544-1564.

Shapiro, L. J., 1983: Asymmetric boundary layer flow under a translating hurricane. *J. Atmos. Sci.*, **40**, 1984-1998.

Smagorinsky, J., S. Manbe, and J. L. Holloway Jr., 1965: Numerical results from a nine-level general circulation model of the atmosphere. *Mon. Wea. Rev.*, **93**, 727-768.

Simpson, R. H., 1952: Exploring the eye of typhoon "Marge" 1951. *Bull. Amer. Meteor. Soc.*, **33**, 286-298.

Wang, B., and X. Li, 1992: The beta drift of three-dimensional vortices: A numerical study. *Mon. Wea. Rev.*, **120**, 579-593.

Wang, Y., 2002a: Vortex Rossby waves in a numerically simulated tropical cyclone. Part I: Overall structure, potential vorticity and kinetic energy budgets. *J. Atmos. Sci.*, **59**, 1213-1238.

—, 2002b: Vortex Rossby waves in a numerically simulated tropical cyclone. Part II: The role in tropical cyclone structure and intensity changes. *J. Atmos. Sci.*, **59**, 1239-1262.

Willoughby, H. E., 1978: A possible mechanism for the formation of hurrican rainbands. *J. Atmos. Sci.*, **47, 242-264**

—, F. D. Marks Jr., and R. J. Feinberg, 1984: Stationary and moving

convective bands in hurricanes. *J. Atmos. Sci.*, **41**, 3189-3211.

Wu, L., 1999: Study of tropical cyclone motion with a coupled hurricane-ocean model. Ph. D dissertation, Department of Meteolorology, University of Hwaii, 212pp.

—, and B. Wang, 2000: A potential vorticity tendency diagnostic approach for tropical cyclone motion. *Mon. Wea. Rev.*, **128**, 1899-1911.

—, and —, 2001a: Movement and vertical coupling of adibatic baroclinic tropical cyclones. *J. Atmos. Sci.*, **58**, 1801-1814.

—, and —, 2001b: Effects of convective heating on movement and vertical coupling of tropical cyclones: A numerical study, *J. Atmos. Sci.*, **58**, 3639-3649.

Table 1: Summary of the numerical experiments

Experiment	Env. Flow	Plane	Heating
E0	NA	f	Diabatic
E1	sheared	f	Diabatic
E2	NA	β	Diabatic
E3	uniform	f	Dibatic

List of Figures

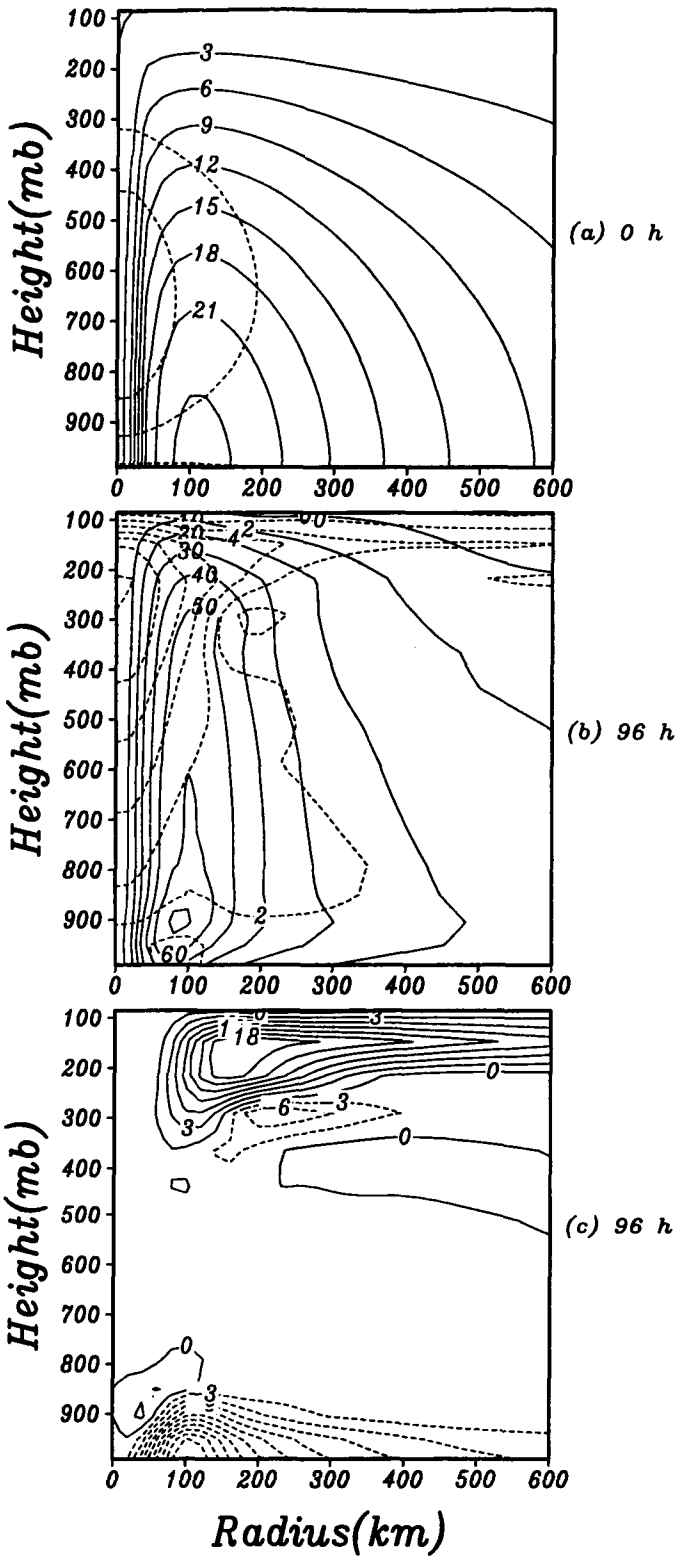

Figure 1: Tangential winds (solid) and temperature anomalies (dashed) with respect to the environment in E0 at 0 h (a) and 96 h (b), and radial winds at 96 h (c). The intervals are 2°C for the temperature anomaly, 3 m/s in (a) and (c) and 10 m/s in (b) for winds.

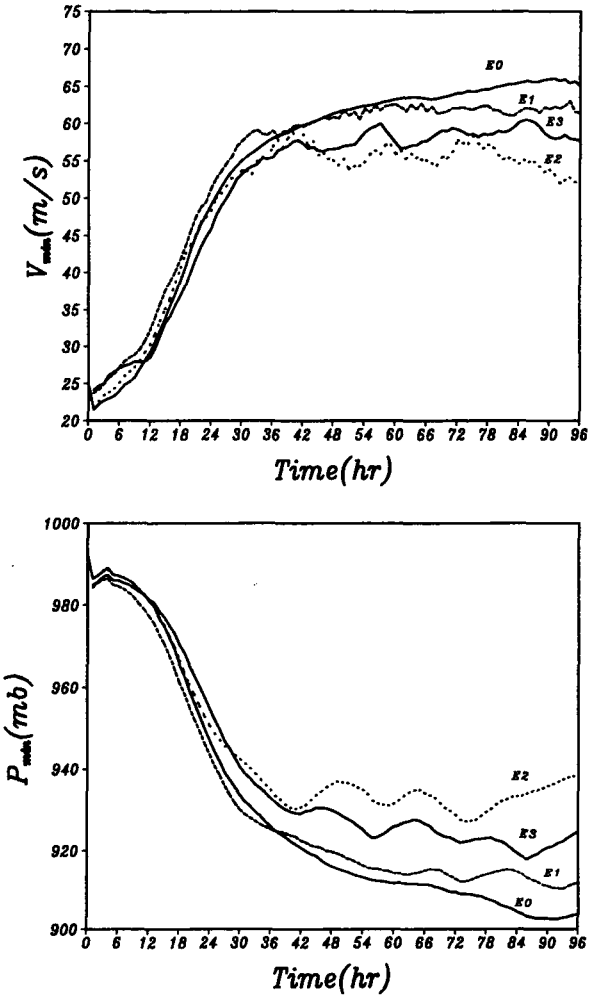

Figure 2: Time series of maximum wind (upper) at the lowest model level and minimum central pressures (lower) for cases E0, E1, E2 and E3.

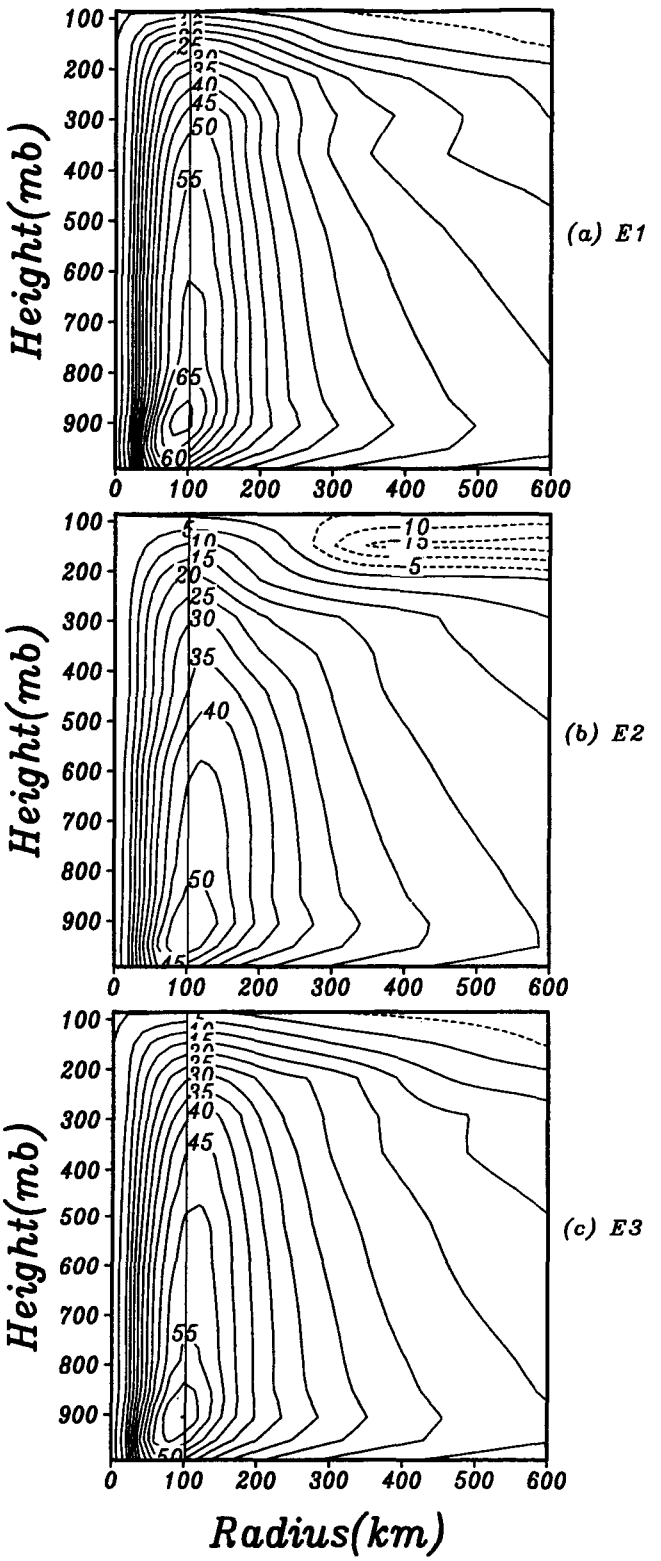

Figure 3: Vertical profiles of the tangential wind in (a) E1, (b) E2 and (c) E3 at 96 h. The intervals are 5 m/s. Vertical lines indicate the location of 100 km.

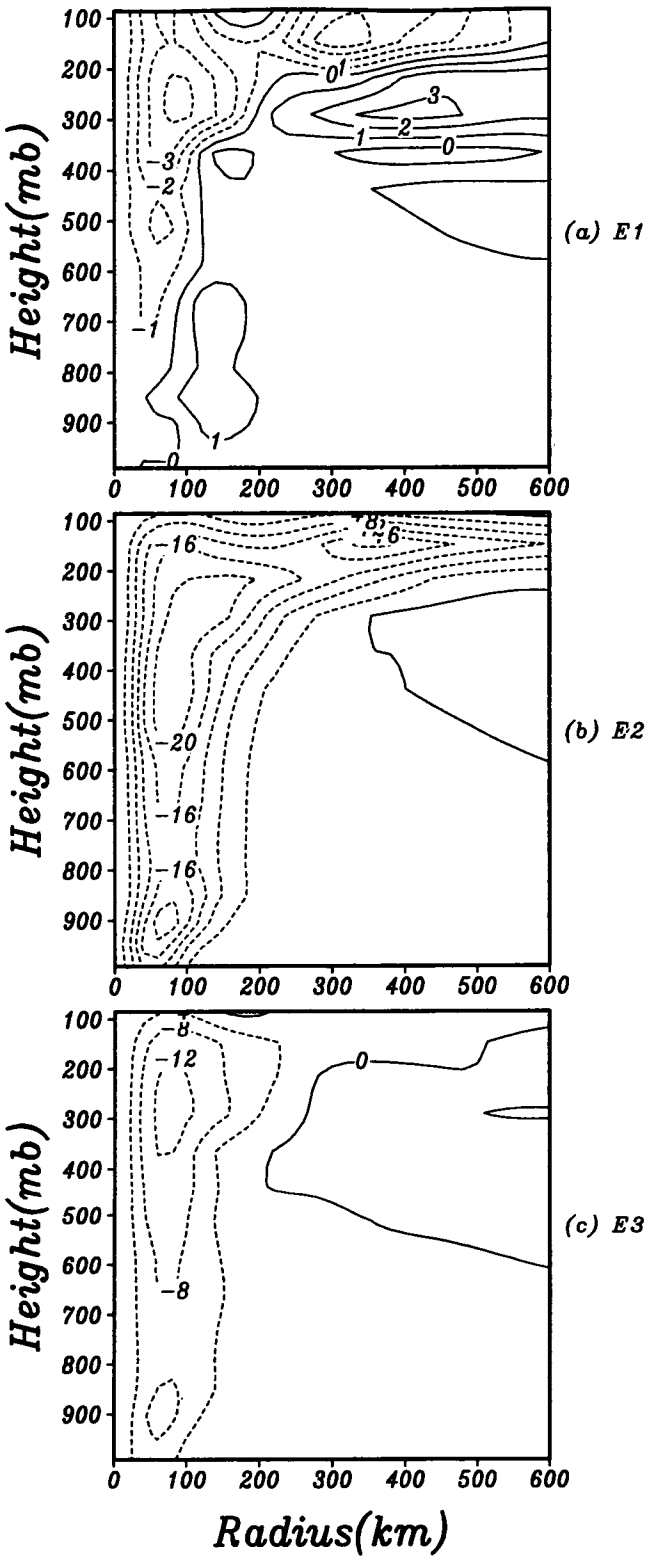

Figure 4: Deviation of the tangential wind in (a) E1, (b) E2 and (c) E3 from that in E0 at 96 h. The intervals are 1 m/s in (a) 4 m/s in (b) and (c), respectively.

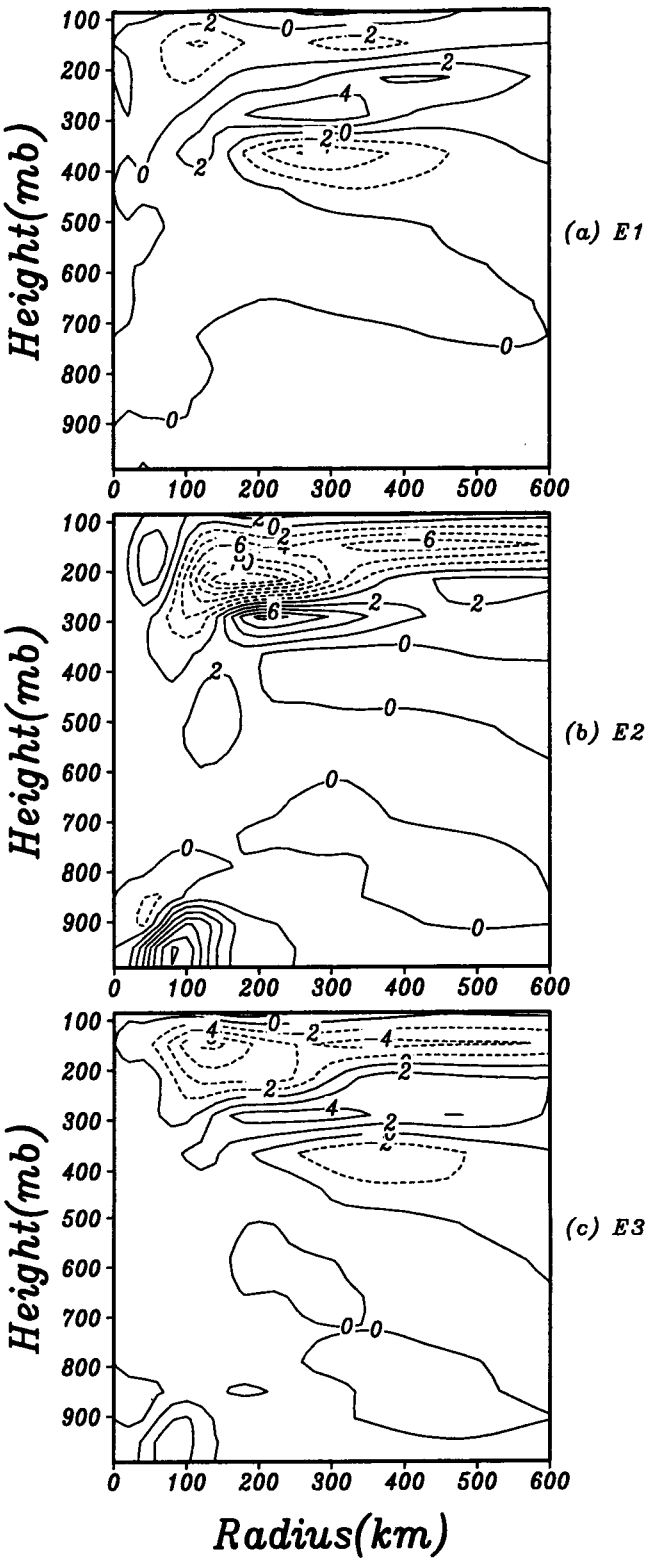

Figure 5: Deviation of the radial winds in (a) E1, (b) E2 and (c) E3 from that in E0 at 96 h. The intervals are 2 m/s.

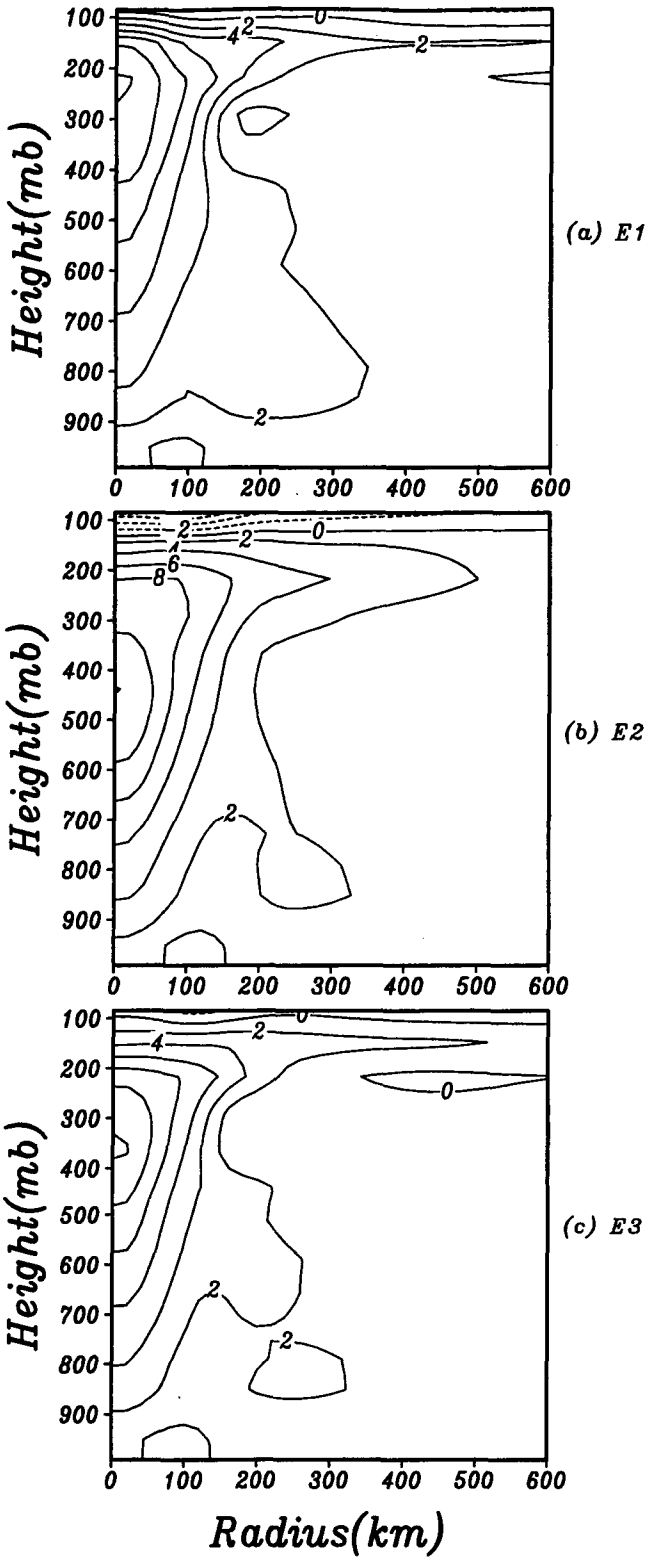

Figure 6: Temperature anomalies relative to the environment in (a) E1 , (b) E2 and (c) E3 at 96 h. The intervals are 2^oC.

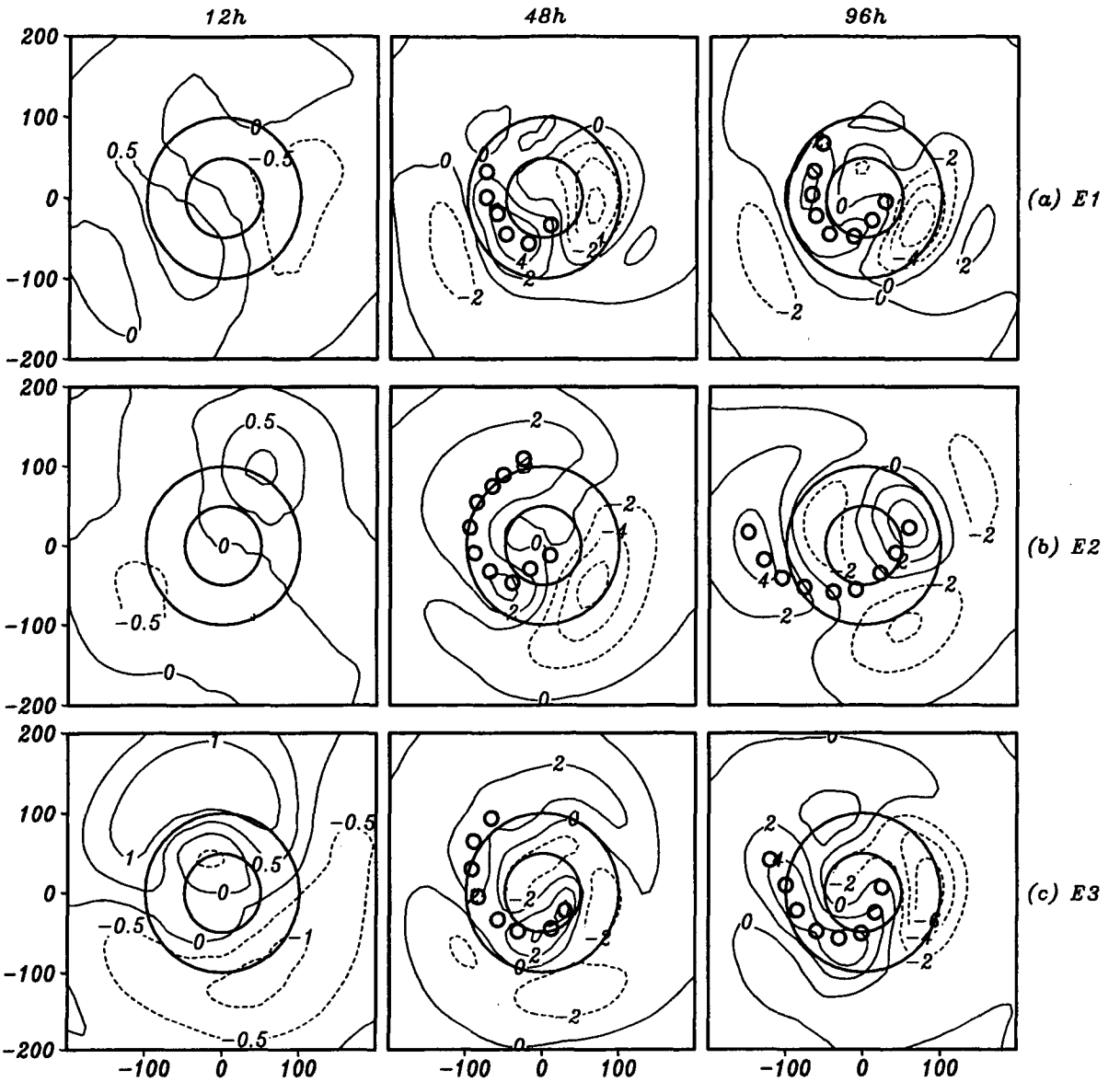

Figure 7: Asymmetric PV components at 900 mb after 12 h, 48 h and 96 h integration in (a) E1, (b) E2 and (c) E3, respectively. The unit for PV is PVU($10^{-6} K m^2 kg^{-1} s^{-1}$). The radii of the two circles are 50 km and 100 km, respectively. Small circles denote the axis of the PV maximum.

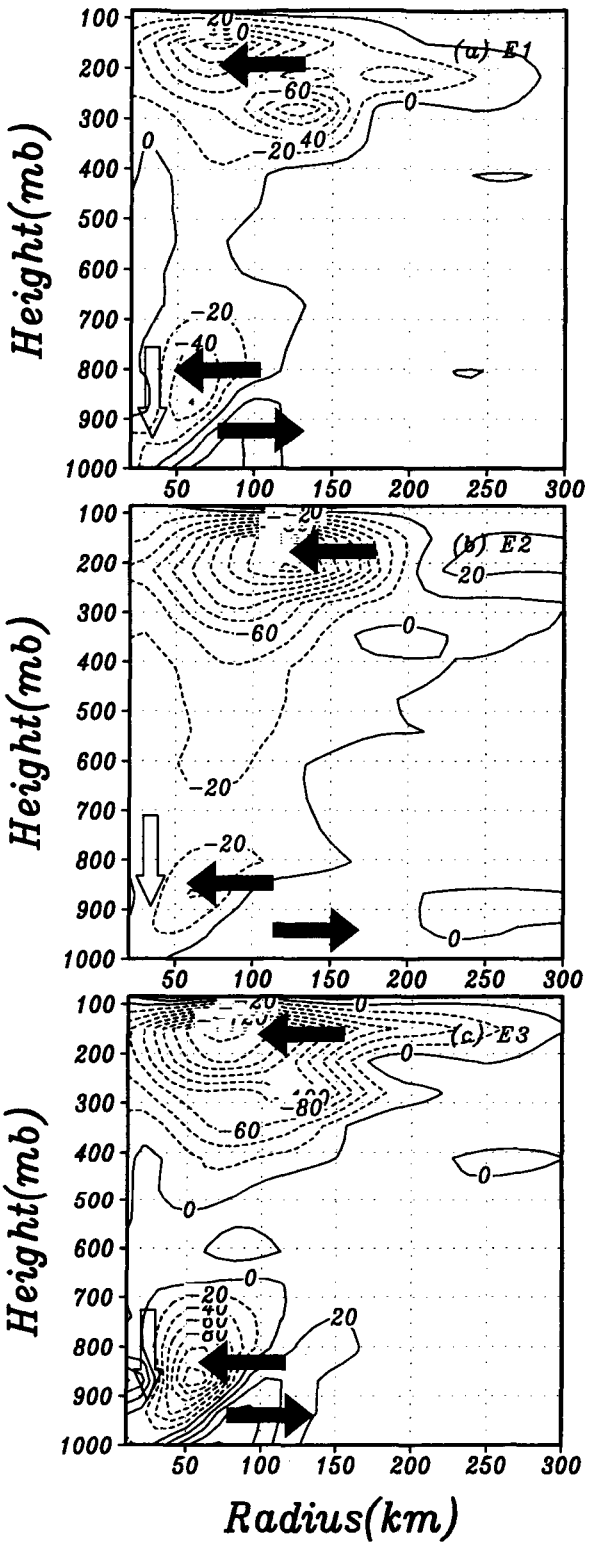

Figure 8: Vertical cross section of the 72 h azimuthal contribution of the asymmetric circulation to the mean radial wind, which is calculated from 24 h to 96 h. Contour intervals are 20 $(ms^{-1})day^{-1}$. The solid arrows schematically show the directions of the induced mean radial flows and the open arrows shows the implied mean downward motion.

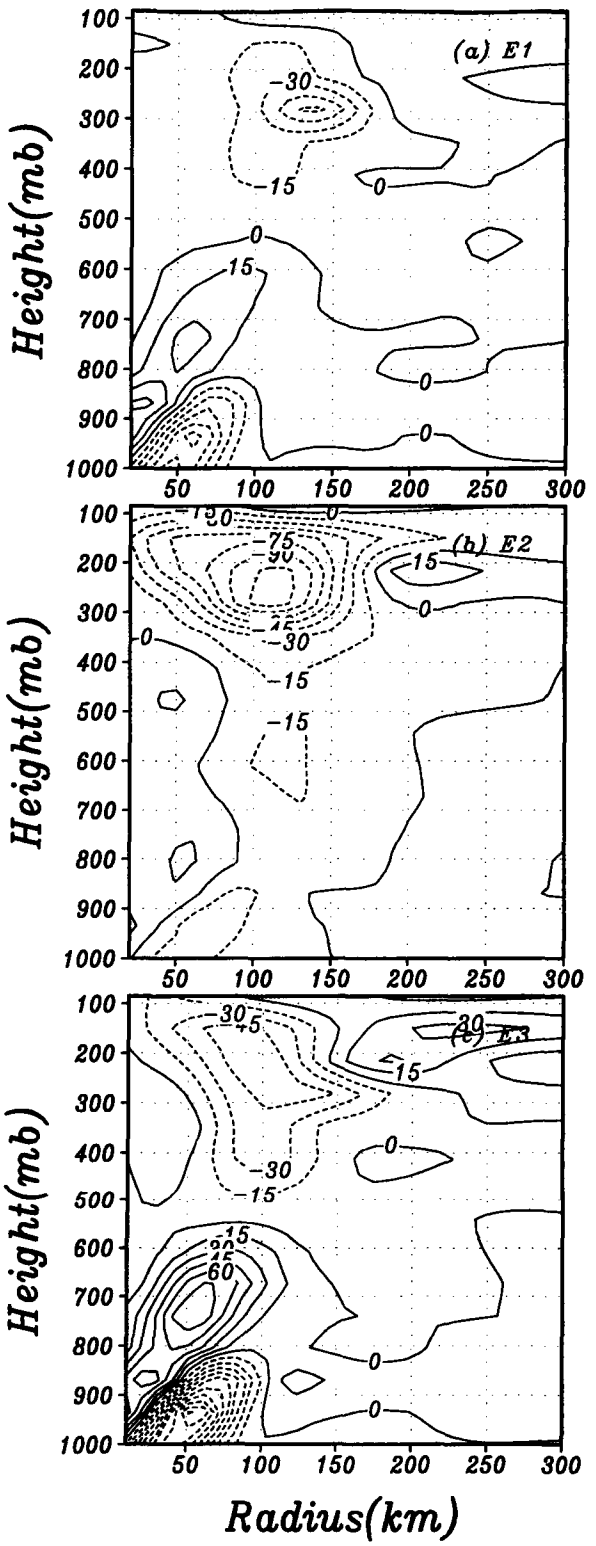

Figure 9: As in Fig. 8 but for the contribution to the mean tangential wind. Contour intervals are 15 $(ms^{-1})day^{-1}$.

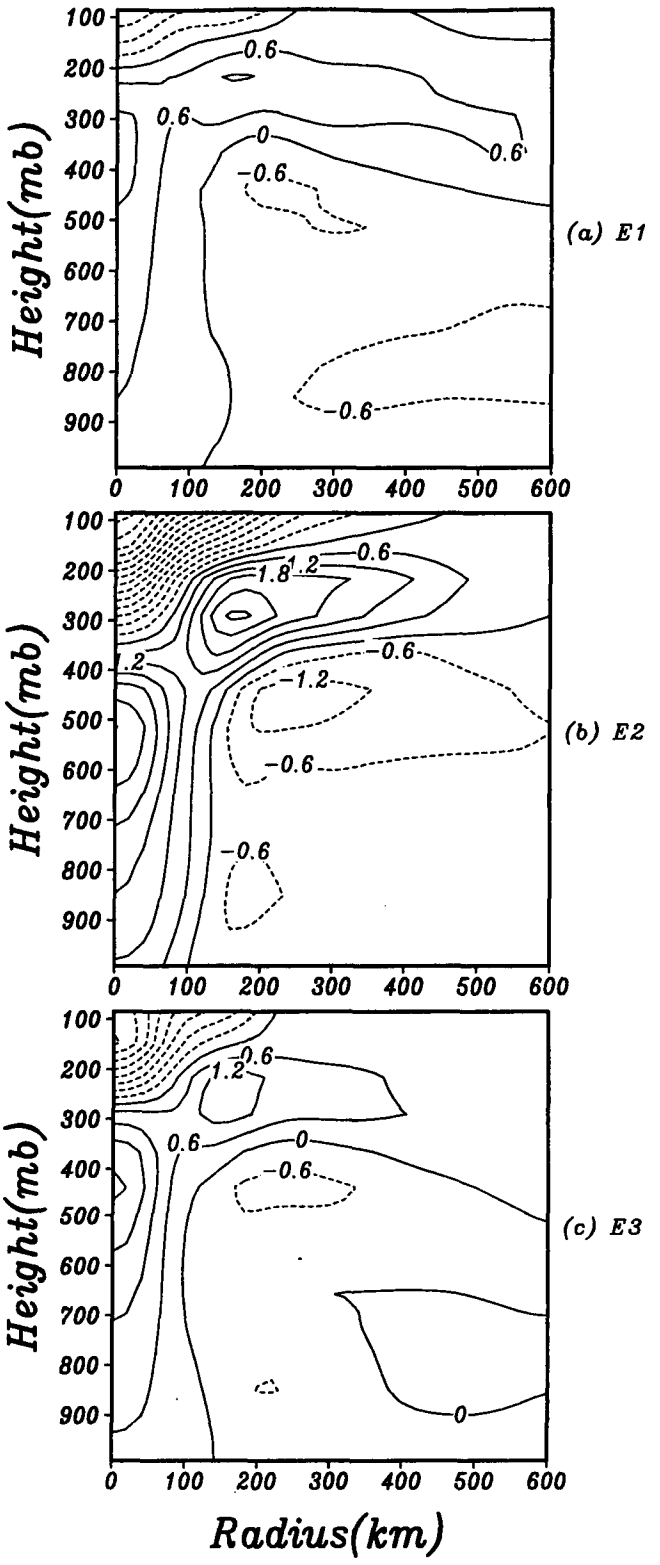

Figure 10: Deviation of temperature in (a) E1 , (b) E2 and (c) E3 from that in E0 at 96 h. The intervals are 0.6^oC.

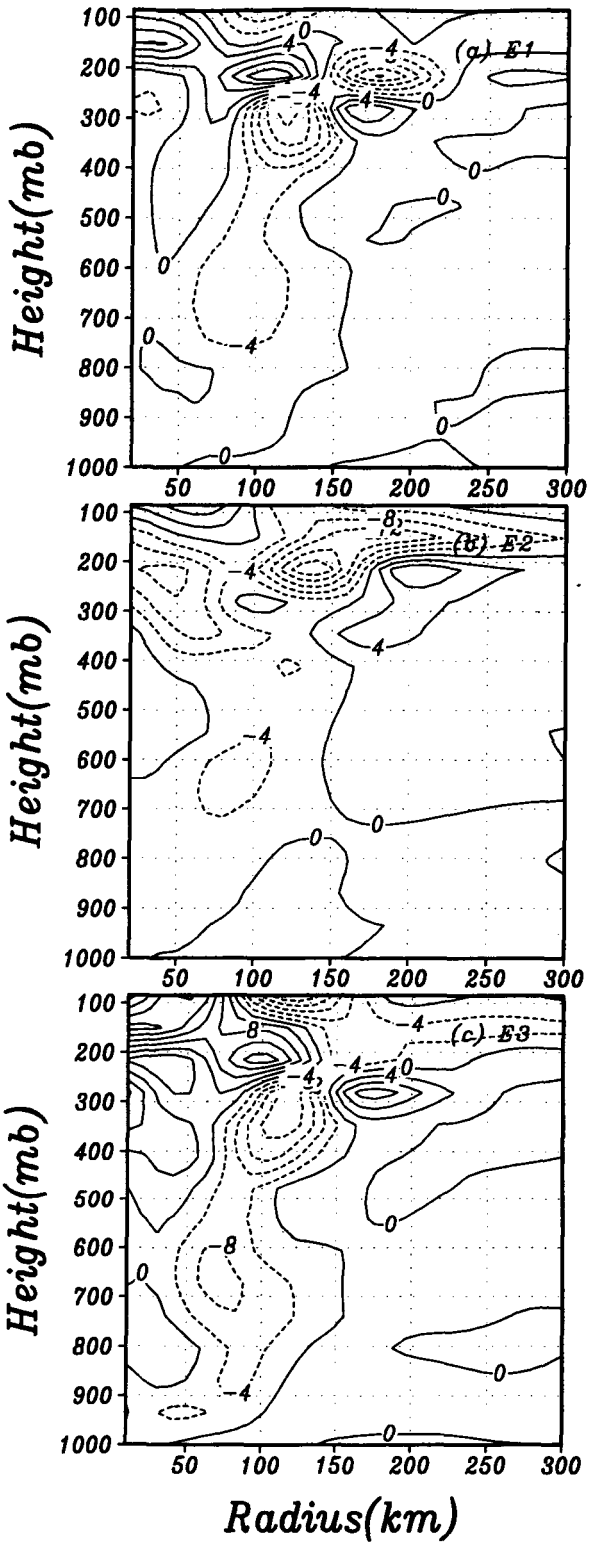

Figure 11: As in Fig. 8 but for the contribution to the mean potential temperature. Contour intervals are 4 $Kday^{-1}$.

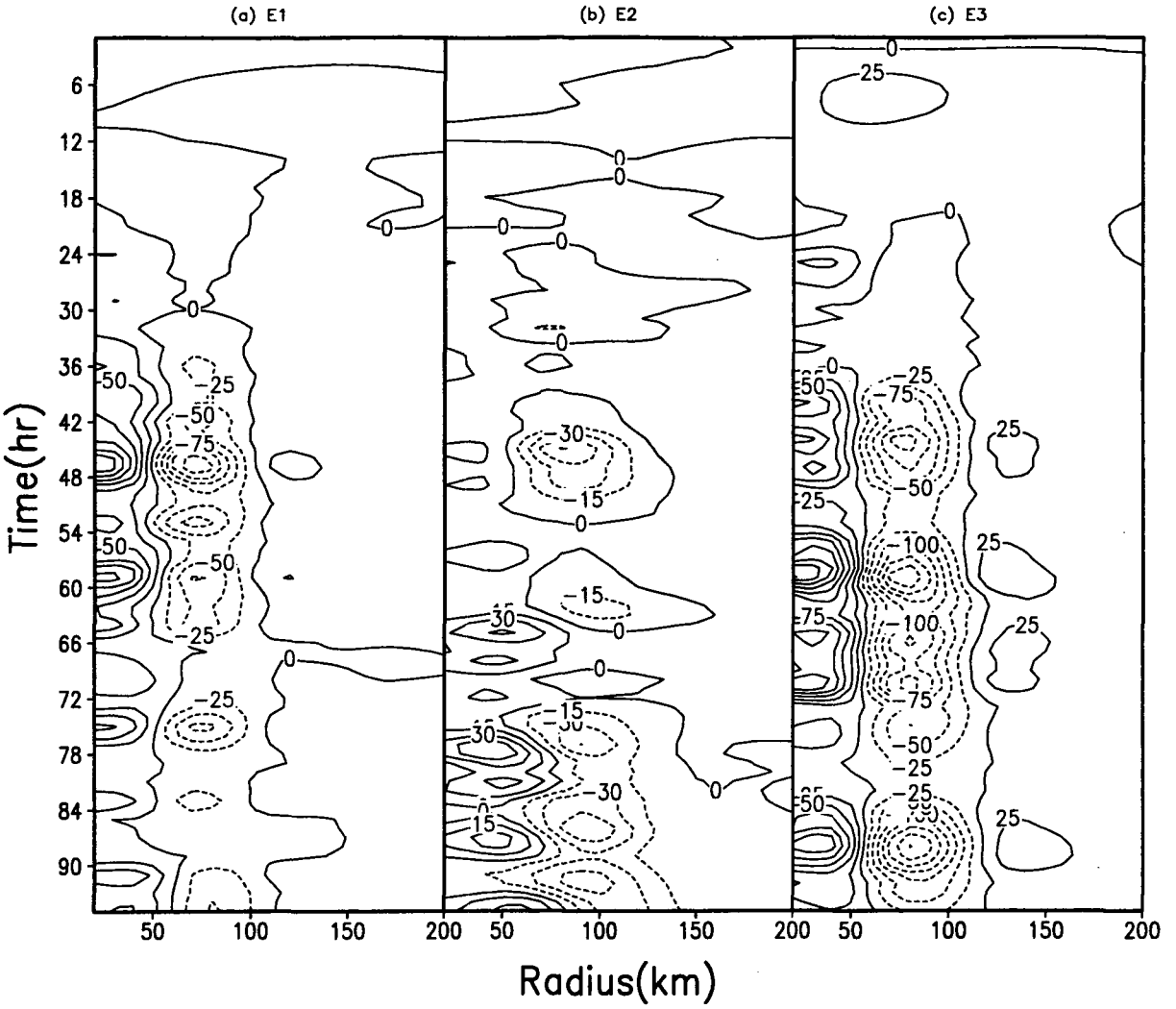

Figure 12: Tendencies of tangential wind associated with the horizontal and vertical momentum fluxes averaged from 24 h to 96 h. Contour intervals are 10 $ms^{-1}day^{-1}$.

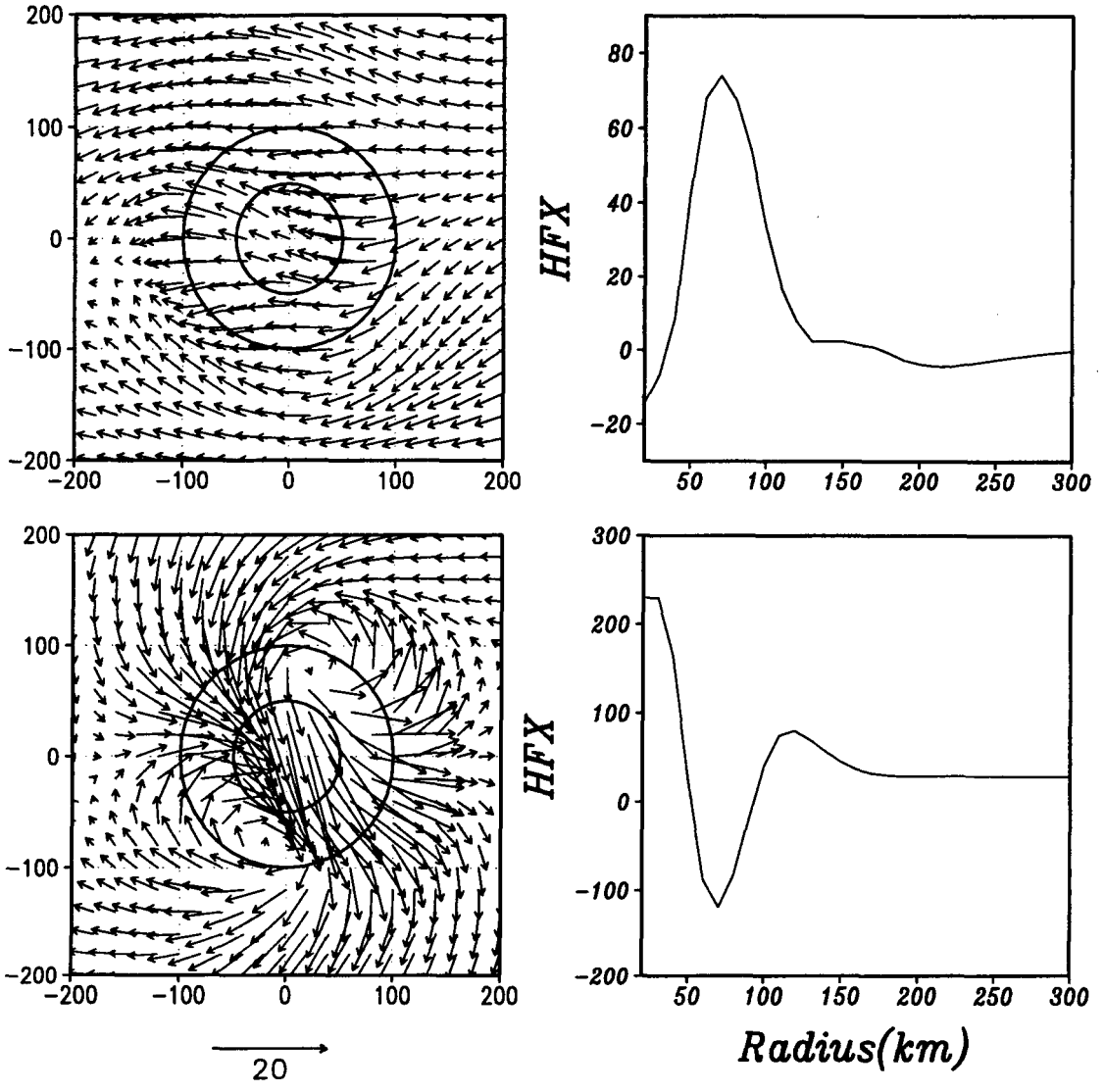

Figure 13: Asymmetric components of the winds(left) and the tendency of tangential wind (right) associated with horizontal momentum flux at 730 and 900 mb nn E3 after 48 h.